Rapid Seismological Quantification of Source Parameters of the 25 April 2015 Nepal Earthquake

by Xiaohui He, Sidao Ni, Lingling Ye, Thorne Lay, Qiaoxia Liu, and Keith D. Koper

ABSTRACT

The 25 April 2015 M_w 7.9 Nepal earthquake is used to explore rapid seismological quantification methods to determine point-source parameters (seismic moment, focal mechanism, radiated energy, and source duration) and rupture directivity parameters (fault length and rupture velocity). Given real-time access to global seismic data, useful results can be obtained from W-phase, energy estimation, cut-and-paste, and backprojection analyses within 20–30 min of origin time or even faster if regional data were openly available (which is not the case at present for stations in China and India). This information can augment ground-shaking prediction procedures such as ShakeMap, which is currently provided by the U.S. Geological Survey National Earthquake Information Center. For such procedures to achieve their full potential, open access to calibrated high-quality ground-motion recordings at local, regional, and global stations is critical, and this should be embraced internationally.

INTRODUCTION

During the last ~10 years, major destructive earthquakes have struck both in oceanic subduction zones (e.g., the great 2004 Sumatra, 2010 Chile, and 2011 Tohoku, Japan, earthquakes), and in continental regions, particularly near margins of the Tibetan plateau (e.g., the 2005 Kashmir, Pakistan, 2008 Wenchuan, China, and 2010 Yushu, China, earthquakes). The 25 April 2015 M_w 7.9 Nepal earthquake (Fig. 1a) once again demonstrated the severe threat that strong seismic events present to society, emphasizing the need for effective earthquake-hazard mitigation efforts. Advances in seismological methods now enable very rapid quantification of faulting in large earthquakes that can guide shaking and tsunami warning systems, identification of regions of large slip and likely damage, and identification of areas of likely aftershock occurrence.

For example, earthquake early warning (EEW) systems are being implemented to exploit fast but relatively weak P waves to issue alerts of incoming strong S-wave or surface-wave shaking, activating immediate efforts to mitigate earthquake damage (Allen and Kanamori, 2003). However, EEW systems require dense seismic instrumentation and advanced data communication networks that are not widely available in developing countries, and they provide as yet limited quantification of the overall earthquake faulting. When a strong earthquake occurs, rapid rescue efforts in the most severely stricken areas can help save the lives of those injured or buried inside collapsed buildings. For this purpose, maps showing the distribution of earthquake fault slip and ground shaking are needed, and such a ShakeMap (Wald *et al.*, 2006) can guide rescue efforts.

Rapid estimation of locations of strong ground shaking requires, at a minimum, fast and reliable estimation of point-source faulting parameters of the earthquake, including magnitude, focal mechanism, and centroid depth. This can potentially be improved by having measures of energy release and source duration, along with finite-source information such as slip distribution, rupture directivity, and identification of the causative fault. Point-source parameters can be determined by moment tensor inversion of seismic waveforms recorded at multiple stations, as routinely performed by the U.S. Geological Survey National Earthquake Information Center (USGS-NEIC) and the Global Centroid Moment Tensor (CMT) project, along with other international efforts. Typically these results are not available within less than 15 min of the origin time because they utilize global seismic-wave observations that may include surface waves that travel relatively slowly. The W-phase moment tensor inversion method (Kanamori and Rivera, 2008; Duputel *et al.*, 2013) uses very-long-period ground motion between the arrivals of the P wave and the fundamental-mode surface waves, so it can provide relatively rapid moment tensors depending on the proximity of open-access broadband stations and their real-time data telemetry. Additionally, the cut-and-paste (CAP) broadband waveform inversion technique has been extended to invert complete local waveforms and/or teleseismic body waves (Zhan *et al.*, 2012; Chen *et al.*, 2015). Because it takes less than 15 min for teleseismic P waves to travel to 95° epicentral distances, CAP inversion of teleseismic P waves can rapidly estimate source parameters. Ground shaking is also related to the source spectrum, stress drop, and total radiated wave energy (e.g., Newman and Okal, 1998; Venkataraman and Kanamori, 2004; Hough, 2014); thus, it is desirable to rapidly estimate total radiated energy for improving prediction of ground shaking,

 doi: 10.1785/0220150131

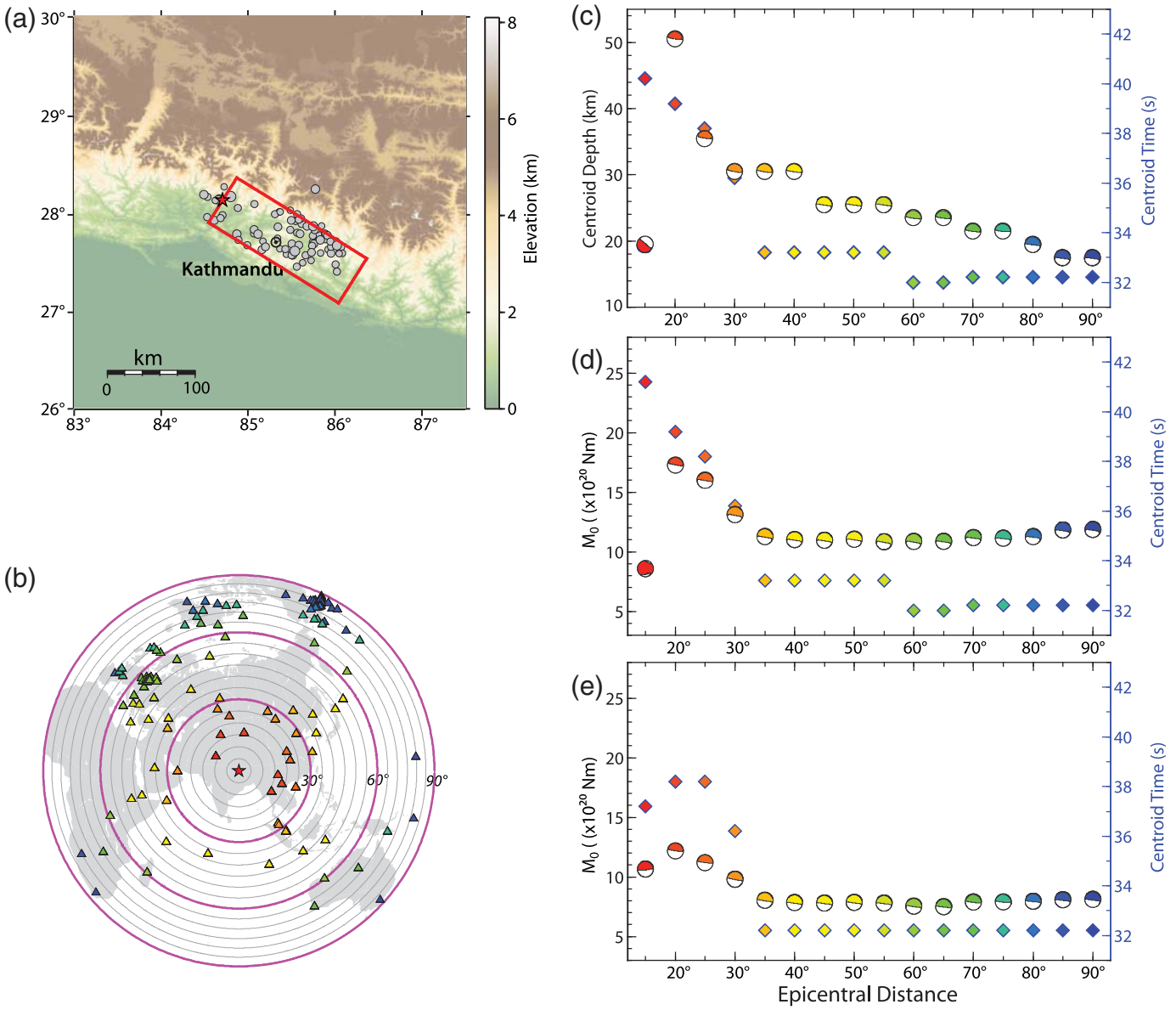

▲ **Figure 1.** (a) The 2015 M_w 7.9 Nepal earthquake epicenter (star) and 1 day aftershocks (circles). The red rectangle indicates approximated ruptured area. (b) Distribution of global seismic stations (triangles, shaded by epicentral distance) used for *W*-phase inversions of three-component ground motions in the 100–600 s period range. (c) Centroid depth estimates (plotted as corresponding focal mechanisms) and centroid time estimates (diamonds) versus maximum epicentral distance within which seismic data are used in *W*-phase inversions. (d, e) Seismic moment M_0 estimates (plotted as corresponding focal mechanisms) and centroid time estimates (diamonds) versus maximum epicentral distance within which seismic data are used in *W*-phase inversions for fixed centroid depths of (d) 9.5 km and (e) 19.5 km.

although more research is needed on how to use radiated energy estimates for local shaking prediction. These source attributes can augment standard ground-motion prediction equation procedures that have been used for a long time (e.g., Hanks and Johnston, 1992).

Finite-source information is also valuable for helping to constrain where strong shaking has occurred, and methods have been developed to rapidly estimate rupture length, rupture velocity, direction of rupture, and slip distribution. Inversions for finite-fault-slip distribution that build on point-source characterization provide the most comprehensive picture of the rupture process (e.g., Ji *et al.*, 2004; Ye *et al.*, 2014), but such inversions usually require human intervention, making near-real-time automation challenging. To reduce the time for estimating first-order rupture directivity parameters, Ammon *et al.* (2006) developed a method of empirical Green's function deconvolution for fundamental-mode Raleigh waves. Similar processing is now applied in near real time to global surface waves using theoretical Green's functions by the Incorporated Research Institutions for Seismology (IRIS); results for

the 2015 Nepal earthquake suggest an eastward propagating rupture (http://ds.iris.edu/spud/sourcetimefunction/9925846, last accessed October 2015).

To reduce the processing time further, it is attractive to use teleseismic *P* waves. Recently, Qin *et al.* (2014) explored the time-shift information in the CAP inversion of local seismic waveforms to compute the difference between centroid location and epicenter, and they resolved the causative fault by fitting azimuthal variations of the time shift, assuming unilateral rupture. Similarly, the time shifts in teleseismic CAP inversions are sensitive to the difference between centroid location and epicenter and can be used to infer rupture directivity parameters. As an alternate approach, the short-period *P*-wave backprojection method has proven effective in imaging expansion of rupture fronts and in resolving rupture length for large earthquakes (e.g., Xu *et al.*, 2009; Yao *et al.*, 2012). Because the backprojection method usually involves teleseismic *P* waves, it can be combined with teleseismic CAP inversion to obtain more robust estimation of rupture directivity parameters. Rupture directivity affects patterns of ground shaking, with strong enhancement for supershear ruptures, so finite-rupture parameters can improve the accuracy of predicted ground-shaking maps.

Here, we use the 2015 Nepal earthquake to demonstrate the potential for rapid seismological characterization of point-source and rupture-finiteness parameters by modeling regional and teleseismic waveforms, using several of the procedures noted above. We consider the evolution of source parameter estimates versus epicentral distance and assess the distance range (time delay after the origin time) needed for reliable source parameter estimation for the specific situation of the Nepal earthquake. Because the tools used in this article are well established, we argue for automation of these software packages to enable construction of improved maps of where strong shaking has occurred within 20–30 min of a large earthquake anywhere in the world. This requires international cooperation and open access to real-time high-quality seismic data from around the world. The Nepal earthquake is an example in which the lack of open access to local, regional, and upper-mantle distance seismic data restricts how quickly earthquake rupture characteristics can be resolved to help guide emergency response efforts. Reducing the time for improved shaking assessment requires open access to more national network data of individual countries.

DATA PROCESSING AND POINT-SOURCE PARAMETER ESTIMATION

We apply procedures here that are used extensively in research programs but could be implemented in operational monitoring facilities. Critical to this rapid analysis is automated event detection and location by national or global monitoring operations such as USGS-NEIC and the continuous acquisition of data from real-time data centers such as the IRIS Data Management System or national data centers. Open access to global seismic stations is critical for this activity, and unfortunately, regional data from national seismic networks in China and India are not openly available in real time for inclusion in rapid analysis procedures or even for delayed analysis. For the 2015 Nepal earthquake source parameter determinations, waveform data with epicentral distances between 10° and 90° were obtained from seismic stations of the Global Seismographic Network (GSN), avoiding clipped data at shorter distances. For CAP analysis, the radial, tangential, and vertical components of ground velocity are obtained after removing any linear trend and instrument response. For backprojection analysis, waveform data at distance between 30° and 95° were obtained from both GSN and regional networks in Alaska, Europe, and Australia.

W-phase inversion has emerged as one of the most robust methods for quickly determining point-source parameters of large earthquakes, and it contributes to the USGS-NEIC ShakeMap production. *W*-phase inversion relies on very-long-period energy (in this case, a 100–600-s-period passband) so is relatively insensitive to Earth structure, and precomputed Green's functions for preliminary reference Earth model work very well. Also, recursive filters are used to remove the instrument response so that even if the later surface-wave arrivals are clipped, as is common at close distances, the signals can be used. We included broadband stations within epicentral distance ranges, increasing in 5° increments, such that the number of stations increases with lapse time from the origin. A similar time-varying process is used by the NEIC automated *W*-phase inversions. Inversion of only the nearest station (NIL, about 11.2° away) gave unstable dip, but by a distance of 20°, six stations provided 10 useful channels yielding a mechanism basically consistent with that for the complete inversion out to 90°. The *W*-phase time window for the 20° range used about 600 s of signal after the origin time, so results could be obtained in about 10 min. Availability of closer stations could reduce this time.

Figure 1 shows that the estimated mechanism is very stable, but centroid depth and centroid time are overestimated for data sets at distances less than 35° (at which point 17 stations with 34 channels are used). If a 19.5 km centroid depth is assumed, based on the tectonic setting, the mechanism is stable at all ranges, but the seismic moment is overestimated before stabilizing with enough data out to a distance of 35°. The *W*-phase data window ends by 1000 s after the origin at 35°, so by 17 min after the event a nearly final solution for mechanism, depth, and seismic moment could have been obtained. Our optimal *W*-phase solution (with 122 stations and 213 channels) has seismic moment 9.09×10^{20} N·m (M_w 7.91), centroid depth 17.5 km, centroid time shift 32.2 s, and best-double-couple nodal plane with strike 287.8°, dip 7.2°, and rake 100°. The NEIC and several other national earthquake monitoring operations have already included routine *W*-phase inversion, but it can be more widely applied in many additional earthquake-monitoring efforts.

We also test reliability of the point-source parameter inversion with teleseismic *P* waves only. We used the CAP joint software (Chen *et al.*, 2015) to invert vertical component *P* waves from 30° to 90° (Fig. 2). A band-pass filter between

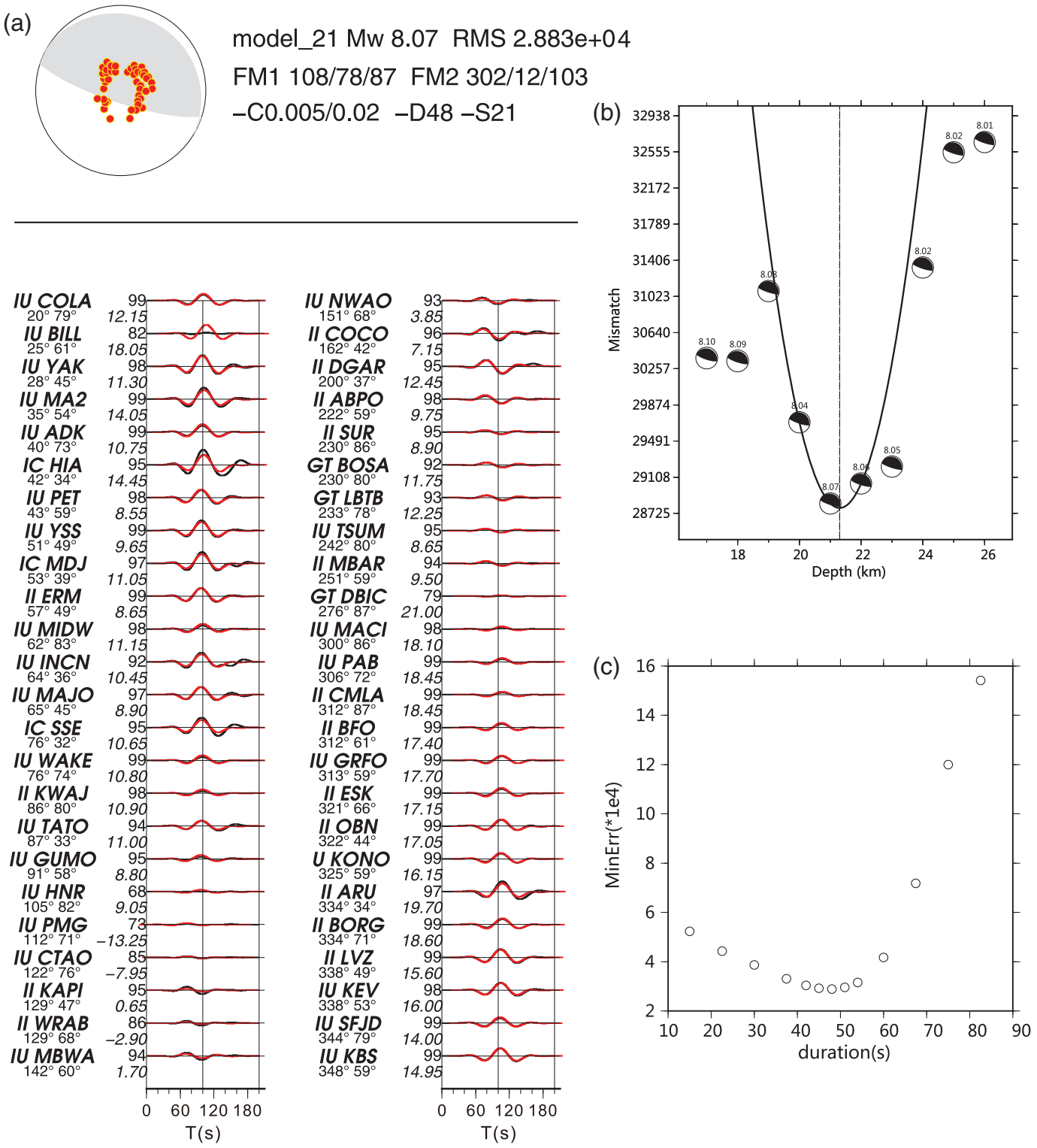

▲ **Figure 2.** (a) Point-source focal mechanism inversion using cut and paste (CAP) for teleseismic *P* waves. Azimuth and epicentral distance are displayed beneath each station code. The red and black traces are synthetic and observed seismograms, respectively. The cross-correlation coefficient (in percentage) and time shift for each station are displayed to the left of each trace pair. (b) CAP waveform inversion mismatch versus centroid depth and (c) waveform mismatch versus source duration.

0.005 and 0.02 Hz was applied to both the observations and the Green's functions. Optimal source duration and centroid depth are grid-searched to minimize waveform mismatch. Compared with the W-phase seismic moment, the CAP inversion yields a somewhat larger size (M_w 8.07), which may be caused by limitations of ray theory for modeling long-period

body waves, differences in the source velocity structure, or differences in fault geometry. The source duration is estimated as ~50 s, close to twice the centroid time of the *W*-phase inversion. The fault-plane solution of CAP has strike 302°, dip 12°, and rake 103°, and a source depth of 21 km. The teleseismic CAP moment tensor inversion provides good overall results; however, for such a long-duration event, the *W*-phase inversion yields more reliable estimates of point-source parameters because it uses a longer-ground-motion time window with multiple phases, longer-period energy, and more complete computation of Green's functions. The CAP waveform inversion procedure can readily be adapted to data at regional and upper-mantle ranges, with suitably precomputed Green's functions, reducing the time required to make source geometry and moment estimates. Hence, CAP can fully exploit increased real-time open access to regional waveforms if more countries provide their data to earthquake-monitoring centers.

Radiated energy can be estimated using teleseismic *P* waves, providing rapid assessments of the seismic energy release from large earthquakes. This is very useful for detecting anomalous events such as tsunami earthquakes. The method of Convers and Newman (2011) is applied in near real time by IRIS; and, for the 2015 Nepal earthquake, IRIS obtained a broadband estimated radiated energy of 7.3×10^{15} J (http://ds.iris.edu/spud/eqenergy/9925797, last accessed October 2015) using 72 global stations. We applied the approach of Venkataraman and Kanamori (2004) and Ye *et al.* (2014) to estimate radiated energy from *P*-wave observations at distances beyond 40° with 5° expanding windows, seeking to assess when sufficient data are available to stabilize the estimate. This procedure requires knowledge of the source depth and focal mechanism of the earthquake, so it must lag behind the point-source inversion for mechanism. Figure 3 summarizes our results, where the station distribution is such that beyond 60° more than 100 stations contribute, leading to stable energy estimates in the $6.0 \pm 0.5 \times 10^{15}$ J range, based on averages from teleseismic *P*-wave spectra. A frequency-dependent attenuation model from Pérez-Campos *et al.* (2003) is used.

The Nepal earthquake has a rather smooth source time function, so a significant percentage of energy was radiated from lower frequency than is stably constrained by the individual *P*-wave spectra. Using the low-frequency spectrum (Fig. 3b) obtained from a finite-fault model with strike 293°, dip 10°, and rake 108° (slightly perturbed from the rapid Global CMT solution), with a rupture expansion velocity of 3.3 km/s (as inferred from backprojections discussed below), increases the energy estimate to 9.75×10^{15} J, as a best broadband estimate up to 2 Hz. The E_R/M_0 ratio is 1.26×10^{-5}, typical of interplate thrust events. These results indicate that an estimate of radiated energy within a factor of 1.6 of the final value could be obtained with 20 min after the event. Radiated energy measures are already applied in some monitoring operations, primarily to detect tsunami earthquake occurrence. Research on how best to utilize the far-field estimates of radiated energy to improve local ground-motion prediction is required.

RUPTURE DIRECTIVITY ESTIMATION FROM CENTROID TIME SHIFTS AND BACKPROJECTION OF TELESEISMIC *P* WAVES

In CAP inversion, the time-shift parameter is caused by a combination of unmodeled lateral variation of velocity structure and the difference between the centroid location and the epicenter assumed in computation of Green's functions. The effect of unmodeled structural variation can be reduced by computing the difference between the centroid time shift and the observed onset time of the *P* wave. The differential time shift displays cosine-like azimuthal variation (Fig. 4). Assuming that major earthquakes tend to rupture mostly unilaterally along strike, rupture length and direction can be inferred from the following equation:

$$\Delta T_i = T_0 + L/(2v) \times \cos(\phi_i - \phi_f), \quad (1)$$

in which ΔT_i is the time shift at station i after correction for onset of the *P* wave; T_0 is the centroid time of the source time function; L is the rupture length, with negative L for rupture along strike; v is the apparent velocity of the teleseismic *P* wave and can be computed from standard 1D Earth models; ϕ_i is the azimuth of station i; and ϕ_f is rupture direction, taken here as the strike of the fault-plane solution of CAP or *W*-phase inversions. Bilateral ruptures will have a more complex azimuthal variation in time shifts that may be quantifiable, but resolution is reduced relative to unilateral cases.

Equation (1) is applied twice to the observed variation of time shifts to avoid bias from strong outliers. That is, the equation is first applied to fit all observations, and a candidate L is obtained. Then the misfit (or residual) at each station is computed, and the overall deviation is calculated. Observations with excessive residual (say the 10% worst residuals) are discarded, and the remaining data are used to estimate rupture length (Fig. 4). The centroid time shift in CAP is measured by cross-correlating observed and synthetic seismograms, thus it may depend on the fault plane used in computing the synthetics. But for the fault-plane solutions from CAP and the *W*-phase inversion (Fig. 4) with data at distances less than 70°, rupture length estimates are consistent (155 versus 151 km), suggesting that a few degree difference in strike and dip does not cause substantial effects. The rupture direction is found to be toward the southeast (from the hypocenter in Fig. 1 toward Kathmandu).

Rupture length estimation was performed for stations within different epicentral distances (Fig. 5). From 40° to 90°, rupture length estimates are quite stable. Over the full range of distances, rupture length is estimated as 175 ± 20 km when the fault-plane solution from CAP inversion is used and 150 ± 20 km when the fault-plane solution from *W*-phase inversion is used. When the centroid time shift is not corrected for *P*-wave onset variations, the rupture length estimates differ by less than 20 km. For stations out to an epicentral distance of 40°, it takes less than 10 min for CAP inversion and 20 min for *W*-phase inversion. Therefore, a good estimate of rupture length could have been obtained within 10–20 min after

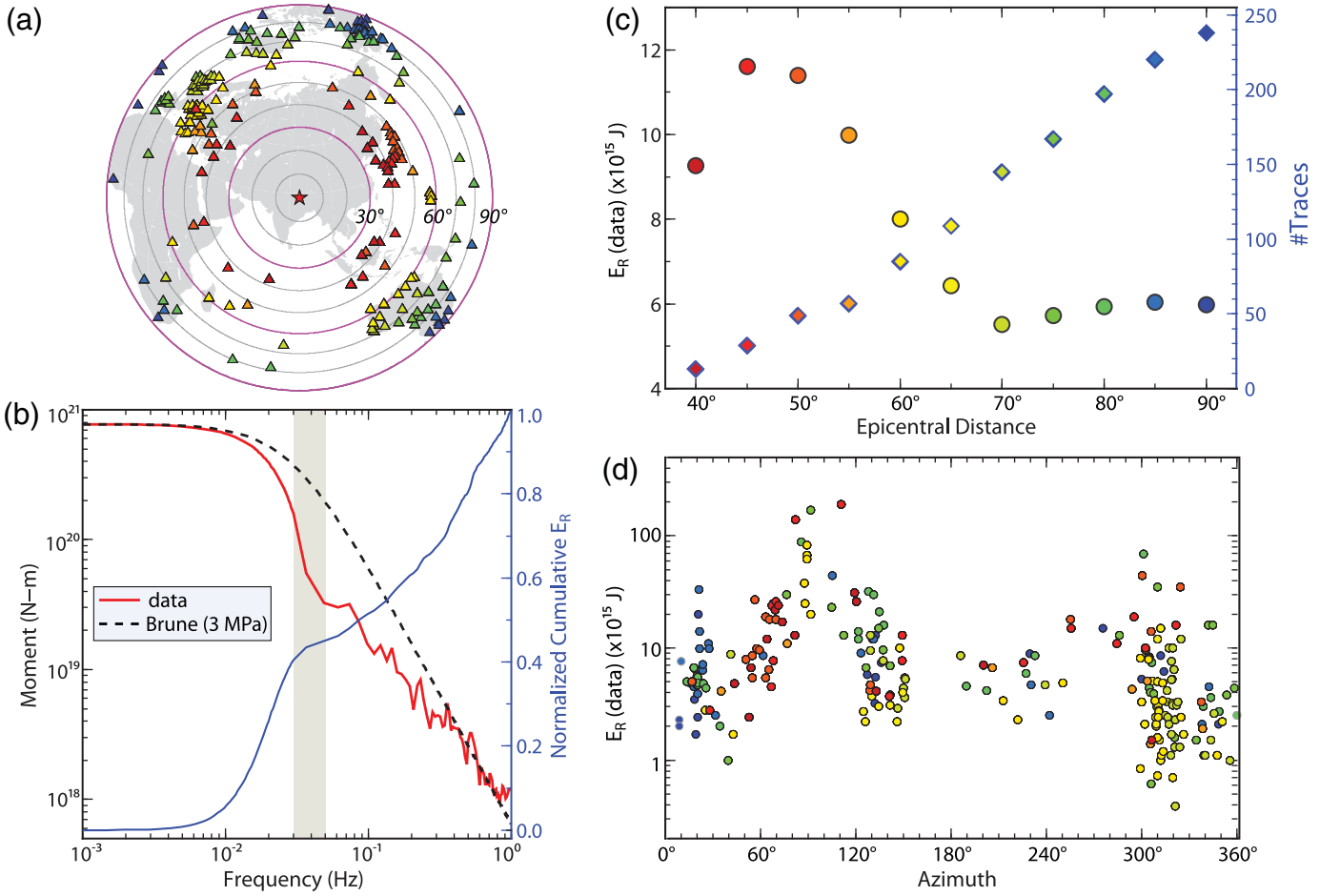

▲ **Figure 3.** Radiated energy E_R estimation. (a) Seismic stations used from 35° to 90° (triangles, colored by distance). The red star represents the epicenter. (b) The average source spectrum (red) of the Nepal earthquake, estimated from a finite-fault inversion for frequencies less than 0.05 Hz and from average spectra of teleseismic *P* waves at higher frequencies, along with the normalized cumulative radiated energy (blue). A reference 3 MPa omega-squared source spectrum for a shear velocity of 3.75 km/s is shown with the dashed line. (c) Estimated radiated energy (circles) and number of traces (diamonds) versus maximum epicentral distance within which seismic data are used. (d) Azimuthal variation of E_R for all stations, with color indicating distance of the station.

the Nepal earthquake began. Rapid access to more regional data could reduce the time for both procedures.

The above rupture directivity parameters are resolved from long-period waveform data. In contrast, backprojection methods use shorter-period *P* waves and can better resolve details of rupture expansion. *P* waves from regional arrays are aligned using multichannel cross correlation (MCCC) of the first 10 s of unfiltered traces (VanDecar and Crosson, 1990). Traces with low-average correlation coefficients are eliminated, and a down-sampling procedure is applied such that only the trace with the highest overall similarity within an ~50 km geographical cell is retained (Fig. 6). For regional arrays in Alaska, Europe, and Australia, short-period *P* energy is backprojected for the Nepal event using the approach of Xu *et al.* (2009) to a 2D grid of points in the source region with uniform spacing of 0.05° in latitude and longitude. The waveforms are bandpassed from 0.5 to 2.0 Hz for the Australia and Europe regions and from 1.0 to 3.0 Hz for the Alaska region. Power is calculated from a tapered, 10-s-long sliding window on a beam that is constructed with fourth-root stacking (Fig. 6). The beam is reconstituted for each 1 s shift in origin time using actual source–receiver distances and MCCC-derived station corrections, so the backprojection times correspond to actual origin times, not relative beam times.

The backprojection results at all three networks show southeastward rupture propagation with a rupture length of about 160–170 km and source duration of 50–55 s, consistent with the rupture directivity estimation from long-period data. The processing described so far can be automated quite reliably. Further processing to remove point-spread array responses from each beam allows peaks to be resolved along the dominant rupture azimuth, and these are combined for several arrays to estimate the overall rupture velocity along that azimuth, which is found to be 3.3 km/s (Fig. 7). This value can then be used to constrain finite-fault model inversions of teleseismic body waves, stabilizing the strong trade-off between rupture velocity and spatial slip distribution. Although in this case we used a late-occurring aftershock to generate an empirical array response

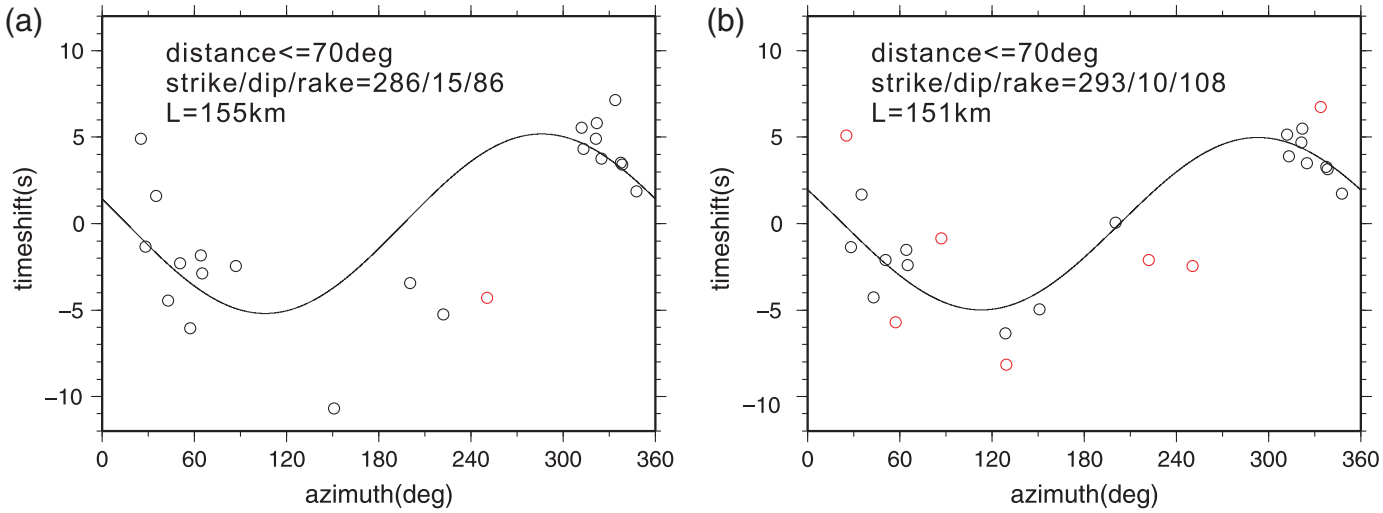

▲ **Figure 4.** Observed (circles) and predicted (solid curve) azimuthal variation of the time shift in equation (1). Red circles indicate outliers with more than 1 sigma deviation. (a) Results using the fault-plane solution from CAP for seismic data with epicentral distances ≤70°. (b) Results using the fault-plane solution from *W* phase for seismic data with epicentral distances ≤70°.

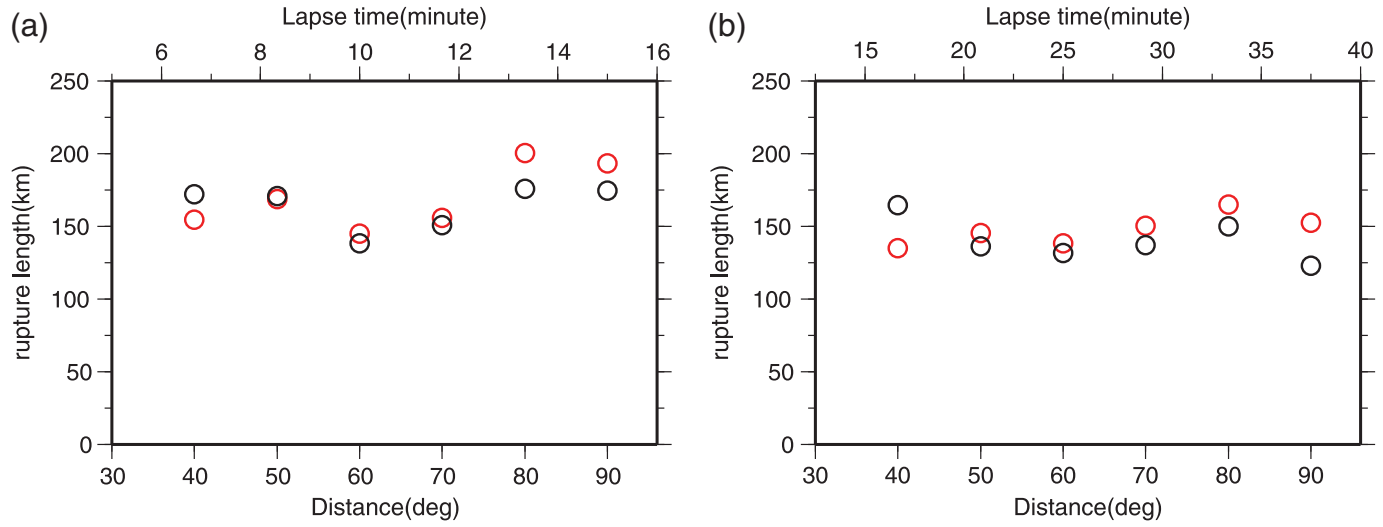

▲ **Figure 5.** Estimates of rupture length versus maximum epicentral distance within which seismic data are used. Red circles represent the rupture length estimates from the differential time between centroid time shift and observed onset time of *P* waves. Black circles represent rupture length estimates based on centroid time shift without correction for *P* onset. (a) Results using the fault-plane solution from teleseismic CAP inversion. (b) Results using the fault-plane solution from *W*-phase inversion.

function, roughly equivalent results can be obtained using ray theory synthetics to simulate the effective array response, but this does not account as reliably for scattering effects and precise attenuation. This processing could potentially be automated but requires some oversight to ensure stability.

DISCUSSION

The backprojection method uses teleseismic *P* waves and does not require a fault-plane solution, so first-order rupture directivity can be estimated within 15 min if the process is automated. One limitation is open-access real-time availability of dense regional networks, but many countries are currently installing or densifying national seismic networks (Zheng *et al.*, 2010). Rupture directivity parameters from the CAP centroid time shift can also be estimated with only teleseismic *P* waves but are more reliable if accurate fault-plane solutions are obtained from *W*-phase inversion. *W*-phase inversion works for regional and teleseismic distances, so availability of broadband real-time data is the major time-limiting factor; and, as soon as enough azimuthally distributed stations are available, good point-source parameters can be estimated. With rapidly obtained accurate point-source and directivity parameters, a more accurate prediction of ground-shaking patterns can be constructed. Even assuming

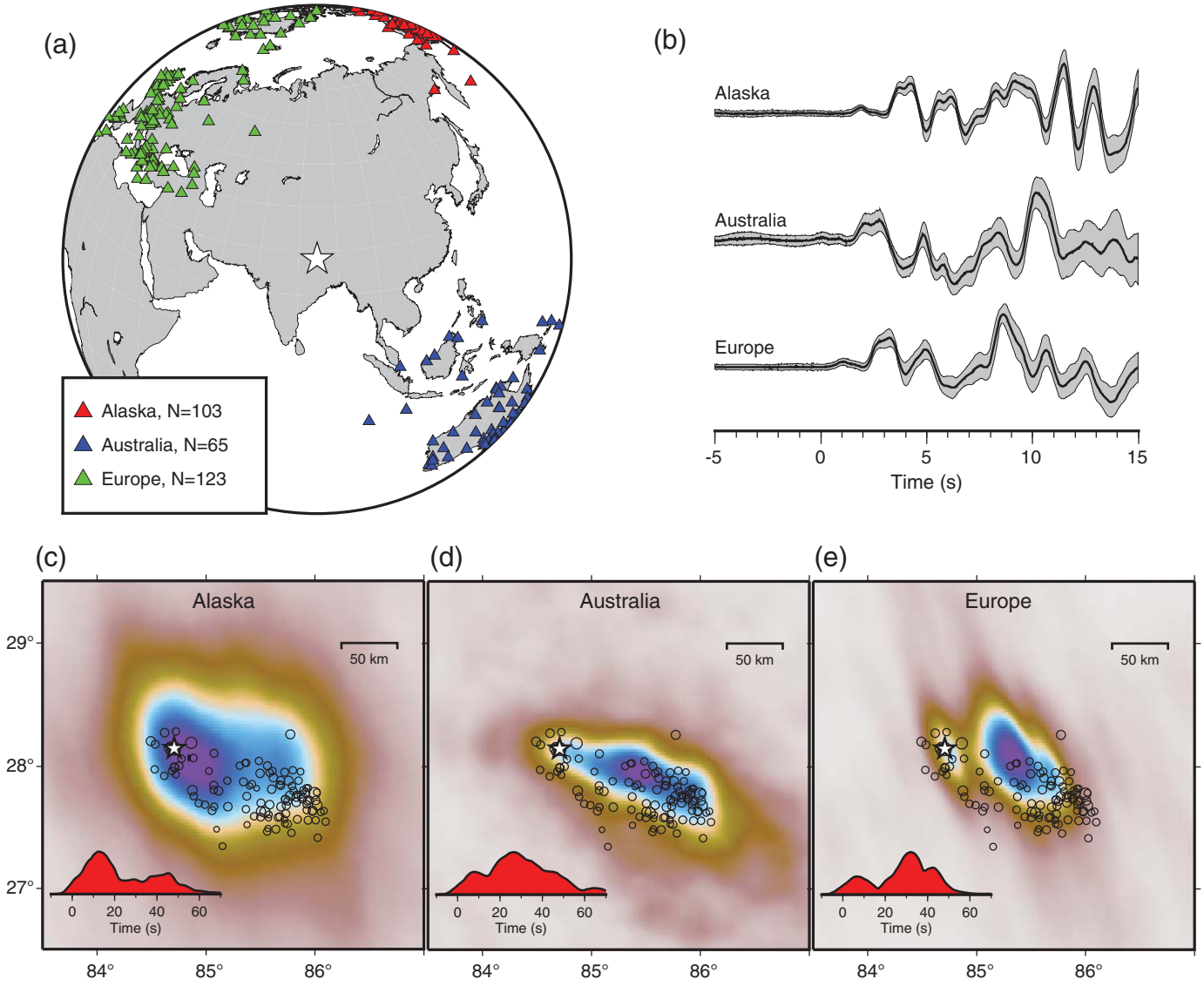

▲ **Figure 6.** (a) Seismic stations (triangles, color coded for three large-aperture networks) used for backprojection imaging. The white star represents the 25 April 2015 Nepal earthquake epicenter. (b) Alignment of initial *P* waves for each of the three arrays. The traces are unfiltered seismograms of ground velocity, with the dark line indicating the array average and the gray region indicating ±1 standard deviation of the waveforms. The bottom panels show time-integrated beam power for backprojections from (c) Alaska, (d) Australia, and (e) Europe. The white star indicates the mainshock epicenter and the circles indicate National Earthquake Information Center (NEIC) locations of aftershocks occurring prior to the M_w 7.3 aftershock of 12 May 2015. The red insets in (c)–(e) show the time evolution of maximum beam power.

a rectangular rupture shape with a typical aspect ratio, the quantitative seismic information should be helpful for emergency response actions involving rapid rescue or in forecasting areas of likely aftershocks (Fig. 1a). Finite-fault inversions with progressively better resolved fault dimensions can be used to update the ground-shaking predictions, as is currently practiced by NEIC.

High-rate Global Positioning System processing can supplement close-in ground-motion recordings, where broadband seismic instruments tend to go off-scale (e.g., Wright *et al.*, 2012). Both the time-varying and static offset information can be analyzed to constrain rupture characteristics if processing is automated. Efforts are needed to improve rapid access to geodetic measures if they are to contribute to rapid faulting quantification.

CONCLUSION

The destructive 25 April 2015 Nepal earthquake provides an opportunity to evaluate various rapid seismological quantification methods to determine point-source parameters (seismic moment, focal mechanism, radiated energy, and source duration) and rupture-directivity parameters (fault length and rupture velocity). With near-real-time access to global seismic data and rapid analyses, useful results can be obtained within

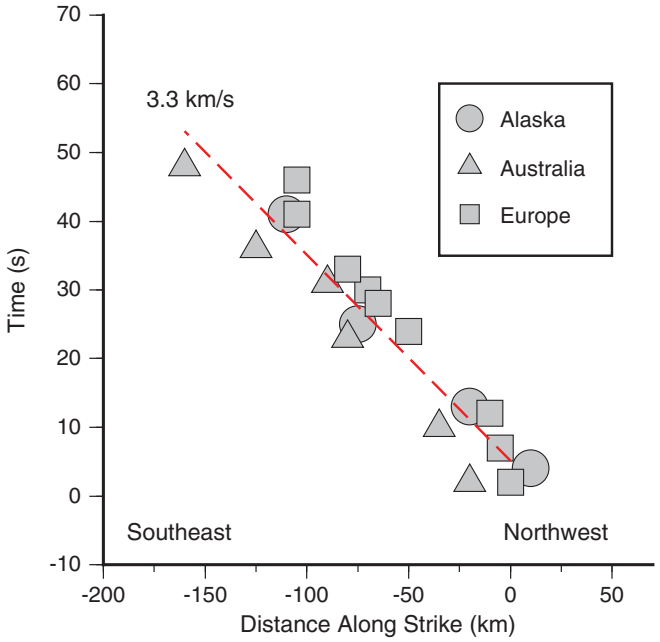

▲ **Figure 7.** Preferred rupture velocity estimate from linear backprojection and deconvolution of empirical array response functions. Symbol size is uniform, and the red dashed line is fit by least-squares regression of unweighted subevent locations.

20–30 min of origin time or even faster. Automation of the tools used here (W phase, energy estimation, CAP, and backprojection) and integration into earthquake detection and location systems needs to be performed for regional and global operations. A few agencies and research programs have automated some procedures. With improved performance of data communication networks, increased coverage of high-rate geodetic networks, and denser national seismic networks, rapid earthquake faulting and ground-shaking quantification can be performed to assist society in responding to future strong earthquakes.

DATA AND RESOURCES

All of the waveform data used in this study are openly available in real time from the Incorporated Research Institutions for Seismology Data Management Center.

ACKNOWLEDGMENTS

This work made use of Generic Mapping Tool (GMT; http://gmt.soest.hawaii.edu/, last accessed October 2015) and Seismic Analysis Code (SAC; http://ds.iris.edu/ds/nodes/dmc/software/downloads/sac/, last accessed October 2015) software. Earthquake locations are from the U.S. Geological Survey National Earthquake Information Center (earthquake.usgs.gov, last accessed June 2015). We thank an anonymous reviewer and Associate Editor Susan Hough for helpful comments on the manuscript. The study is supported by National Natural Science Foundation of China (NSFC) funding (4146116400, to S. N. and H. H.) and National Science Foundation (NSF) Grant EAR-1245717 (to T. L.). Q. L. is also supported by the China Scholarship Council (CSC) Overseas Scholar Program.

REFERENCES

Allen, R. M., and H. Kanamori (2003). The potential for earthquake early warning in southern California, *Science* **300,** 786–789.

Ammon, C. J., A. A. Velasco, and T. Lay (2006). Rapid estimation of first-order rupture characteristics for large earthquakes using surface waves: 2004 Sumatra-Andaman earthquake, *Geophys. Res. Lett.* **33,** L14314, doi: 10.1029/2006GL026303.

Chen, W., S. Ni, H. Kanamori, S. Wei, Z. Jia, and L. Zhu (2015). CAPjoint, a computer software package for joint inversion of moderate earthquake source parameters with local and teleseismic waveforms, *Seismol. Res. Lett.* **81,** 432–441.

Convers, J. A., and A. V. Newman (2011). Global evaluation of large earthquake energy from 1997 through mid-2010, *J. Geophys. Res.* **116,** no. B08304, doi: 10.1029/2010JB007928.

Duputel, Z., V. C. Tsai, L. Rivera, and H. Kanamori (2013). Using centroid time delays to characterize source durations and identify earthquakes with unique characteristics, *Earth Planet Sci. Lett.* **375,** 92–100, doi: 10.1016/j.epsl.2013.05.024.

Hanks, T. C., and A. C. Johnston (1992). Common features of the excitation and propagation of strong ground motion for North American earthquakes, *Bull. Seismol. Soc. Am.* **82,** 1–23.

Hough, S. E. (2014). Shaking from injection-induced earthquakes in the central and eastern United States, *Bull. Seismol. Soc. Am.* **104,** 2619–2626, doi: 10.1785/0120140099.

Ji, C., D. V. Helmberger, and D. J. Wald (2004). A teleseismic study of the 2002 Denali, Alaska, earthquake and implications for rapid strong motion estimation, *Earthq. Spectra* **20,** 617–637.

Kanamori, H., and L. Rivera (2008). Source inversion of W phase: Speeding up seismic tsunami warning, *Geophys. J. Int.* **175,** 222–238.

Newman, A. V., and E. A. Okal (1998). Teleseismic estimates of radiated seismic energy: The E/M_0 discriminant for tsunami earthquakes, *J. Geophys. Res.* **103,** no. B11, 26,885–26,898, doi: 10.1029/98JB02236.

Pérez-Campos, X., S. K. Singh, and G. C. Beroza (2003). Reconciling teleseismic and regional estimates of seismic energy, *Bull. Seismol. Soc. Am.* **93,** 2123–2130.

Qin, L. B., W. W. Chen, S. Ni, L. B. Han, and Y. Luo (2014). A method of resolving earthquake rupture directivity with relative centroid location and its application to the 2008 Yingjiang M_s 6.0 earthquake, *Chin. J. Geophys.* **57,** 3259–3269, doi: 10.6038/cjg20141014 (in Chinese)

VanDecar, J. C., and R. S. Crosson (1990). Determination of teleseismic relative phase arrival times using multi-channel cross-correlation and least squares, *Bull. Seismol. Soc. Am.* **80,** 1548–1560.

Venkataraman, A., and H. Kanamori (2004). Observational constraints on the fracture energy of subduction zone earthquakes, *J. Geophys. Res.* **109,** no. B05302, doi: 10.1029/2003JB002549.

Wald, D. J., P. S. Earle, K. Lin, V. Quitoriano, and B. C. Worden (2006). Challenges in rapid ground motion estimation for the prompt assessment of global urban earthquakes, *Bull. Earthq. Res. Inst.* **81,** 275–283.

Wright, T. J., N. Houlié, M. Hildyard, and T. Iwabuchi (2012). Real-time, reliable magnitudes for large earthquakes from 1 Hz GPS precise point positioning: The 2011 Tohoku-Oki (Japan) earthquake, *Geophys. Res. Lett.* **39,** L12302, doi: 10.1029/2012GL051894.

Xu, Y., K. D. Koper, O. Sufri, L. Zhu, and A. R. Hutko (2009). Rupture imaging of the M_w 7.9 12 May 2008 Wenchuan earthquake from

back projection of teleseismic *P* waves, *Geochem. Geophys. Geosyst.* **10,** Q04006, doi: 10.1029/2008GC002335.

Yao, H. J., P. Shearer, and P. Gerstoft (2012). Subevent location and rupture imaging using iterative backprojection for the 2011 Tohoku M_w 9.0 earthquake, *Geophys. J. Int.* **190,** 1152–1168, doi: 10.1111/j.1365-246X.2012.05541.x.

Ye, L., T. Lay, K. D. Koper, R. J. Smalley, L. Rivera, M. Bevis, A. Zakrajsek, and F. Teferle (2014). Complementary slip distributions of the August 4, 2003 M_w 7.6 and November 17, 2013 M_w 7.8 South Scotia Ridge earthquakes, *Earth Planet. Sci. Lett.* **401,** 215–226, doi: 10.1016/j.epsl.2014.06.007.

Zhan, Z., D. Helmberger, M. Simons, H. Kanamori, W. Wu, N. Cubas, Z. Duputel, R. Chu, V. C. Tsai, J.-P. Avouac, *et al.* (2012). Anomalously steep dips of earthquakes in the 2011 Tohoku-Oki source region and possible explanations, *Earth Planet. Sci. Lett.* **353/354,** 121–133, doi: 10.1016/j.epsl.2012.07.038.

Zheng, X. F., Z. X. Yao, J. H. Liang, and J. Zheng (2010). The role played and opportunities provided by IGP DMC of China National Seismic Network in Wenchuan earthquake disaster relief and researches, *Bull. Seismol. Soc. Am.* **100,** 2866–2872.

Xiaohui He
Qiaoxia Liu[1]
School of Earth and Space Sciences
University of Science and Technology of China
Hefei 230026, China
hexiaohu@mail.ustc.edu.cn
liuqx083@mail.ustc.edu.cn

Sidao Ni
State Key Laboratory of Geodesy and Earth's Dynamics
Institute of Geodesy and Geophysics
Chinese Academy of Sciences
Wuhan 430077, China
sdni@whigg.ac.cn

Lingling Ye
Thorne Lay
Earth and Planetary Sciences Department
University of California, Santa Cruz
Santa Cruz, California 95064 U.S.A.
lye2@ucsc.edu
tlay@ucsc.edu

Keith D. Koper
Department of Geology and Geophysics
University of Utah
Salt Lake City, Utah 84112 U.S.A.
koper@seis.utah.edu

[1] Also at Department of Geology and Geophysics, University of Utah, Salt Lake City, Utah 84112 U.S.A.